Solar Energy 160 (2018) 94–102

Contents lists available at ScienceDirect

Solar Energy

journal homepage: www.elsevier.com/locate/solener

Saharan dust transport to Europe and its impact on photovoltaic performance: A case study of soiling in Portugal

Ricardo Conceição[a,*], Hugo G. Silva[a], José Mirão[b], Michael Gostein[c], Luis Fialho[a], Luis Narvarte[d], Manuel Collares-Pereira[a]

[a] Renewable Energies Chair, University of Évora, Portugal
[b] Hercules Laboratory, University of Évora, Portugal
[c] Atonometrics Inc., TX, United States
[d] Universidad Politécnica de Madrid, Spain

ARTICLE INFO

Keywords:
Solar energy
Saharan desert dust transport
Soiling
Photovoltaic performance

ABSTRACT

The impact of long range Saharan dust transport, arising from one event in February and other in March 2017, on the performance of photovoltaic flat panels is reported as a case study of soiling. Through satellite images, dust coming from north Africa was detected, while using the Hybrid Single-Particle Lagrangian Integrated Trajectory, specific origin locations of the dust were found. Dust accumulated on glass coupons deployed in Southern Portugal, Évora and Alter do Chão, was analysed by Scanning Electron Microscopy and Energy Dispersive X-ray Spectroscopy. Mass accumulation on those coupons was weekly measured with a microbalance and related with environmental parameters, aerosol optical depth and rain, through a proposed empirical model. Performance measurement took place at Évora using mc-Si PV flat panels and an I-V curve tracer to get two parameters: maximum output power and short-circuit current. It was found that the first dust event led to decreases in the maximum output power of ≈8% and in the short-circuit current of ≈3%, while the second event led to a decrease of ≈3% in both parameters. A relation between PV performance and mass accumulation was successfully explored.

1. Introduction

Soiling, defined as particle deposition on surfaces, reduces a PV cell's incoming radiation by reflecting it back to the atmosphere or absorbing it. The amount of soiling and how it is spread along the surface of the PV panel is geography and time dependent, which means soiling will vary from site to site. This fact is easy understandable, since different locations may have different climates, which implicates different meteorological conditions, like temperature, relative humidity, rain, wind speed and direction (Sayyah et al., 2014), that affect the way particles adhere to surfaces (Kazmerski et al., 2016). Moreover, different locations may have different types of particles suspended in the atmosphere, which also might have a different effect on how and to what extend the radiation entering the panels will be reduced (El-Shobokshy and Hussein, 1993; Appels et al., 2013). Even neighbor locations may have different types and amounts of soiling, depending if they are close to a specific source of particles, e.g. factories, airports and roads, among others (Mejia and Kleissl, 2013). Though most of those studies were done in or near desert areas, where soiling is a major problem (Mallineni et al., 2014) and where there are high values of solar energy availability. However, there are other locations with huge potential for solar energy usage that also need attention regarding soiling and where it can also be problematic, as will be shown, Portugal being one of these cases. This country is one of the best to deploy solar energy harvesting technologies in Europe (Šúri et al., 2007); its southern region has annual availabilities of global horizontal irradiation that can go up to approximately 1800 kW h/m^2, (Lopes et al., in preparation). With such availability, it is therefore expected that solar technologies, such as PV, will be very common in Portugal in the future, which makes soiling an interesting and very important factor to be taken into account. Besides that, it is also an objective to understand and explain phenomena like the ones documented here and draw conclusions that may in fact be used in future studies. Also taking into account the latest NASA Earth Exchange Global Daily Downscaled Projections (NEX-GDDP) (Thrasher et al., 2012; Sheffield et al., 2006), in 2100 this region will have higher air temperatures than at the present time and it will rain less frequently but with more intensity, which are negative projections regarding soiling, since if they become a reality,

* Corresponding author.
E-mail address: rfc@uevora.pt (R. Conceição).

https://doi.org/10.1016/j.solener.2017.11.059
Received 22 September 2017; Received in revised form 13 November 2017; Accepted 22 November 2017
Available online 22 December 2017

there will be more time for particles to build up on the surfaces, leading to an increased soiling over time. Moreover, if climate change follows this trend, Southern Portugal and Spain will become semi-arid regions, which can also lead to an increase of particles suspended in the atmosphere that are able to deposit, because vegetation acts as a particle retainer and obstacle (Smith, 1977).

In this context, Saharan desert dust storms are a significant source of dust, that frequently reach Portugal (around 4–5 major events per year) (Flentje et al., 2015), bringing quantities of dust that significantly influence the performance of PV systems, as will be shown. In fact, during this study a major Saharan desert dust storm took place on 20th–24th February 2017, in which a large amount of dust was swept up into a low pressure system over North Africa, leading to the transportation of a dust cloud over Portugal. Significant soiling was detected and it was derived mainly not from local particles, but from the ones with very far away origin. Though with less intensity, another dust event occurred on March 2017 from 14th–16th and it is also documented here. This work points towards the fact that not only local environment affects soiling, but it shows instead that long-range dust transport (from a process developed thousands of kilometres away) can also influence soiling and the PV performance on a far away region. This work uses the mentioned Saharan desert events as a case study to highlight the importance of these phenomena in the energy production of the region and also the need to develop mitigation tools, e.g., proper dust storm forecasts or the use of active and passive cleaning mechanisms.

2. Experimental setup

Soiling measurements took place at two rural locations in Southern Portugal (Alentejo): Évora at Plataforma de Ensaios de Coletores Solares (PECS) facilities from the Renewable Energies Chair (CER) (Horta et al., 2015) and Alter do Chão in a 200 ha olive tree property of Elaia group (ELAIA) with the following coordinates: Évora - 38°34′0.01″ N; 7°54′0.00″ W and Alter do Chão - 39°12′3.39″ N; 7°39′37.09″ W. The glass sample at this location is part of a larger soiling experiment of the European project MArket uptake of an innovative irrigation Solution based on LOW WATer-ENergy consumption (MASLOWATEN funded by Horizon 2020, contract number 640771). The MASLOWATEN project, in which CER participates, is led by Universidad Politécnica de Madrid and its objective is to use high power PV pumping systems for productive agriculture irrigation consuming zero conventional electricity and achieving less water consumption.

2.1. Mass accumulation

SINA high transmittance solar glass coupons, from Interfloat Corporation, were left outdoors in two experimental setups. In PECS, the experimental setup consists of 25 coupons, with 11 cm length 9 cm width and 3.2 mm thickness at approximately 1.5 m height from the ground, with 6 samples per geographical direction (North, East, South and West) in 15° inclination steps and one completely horizontal on the top, following the idea in Elminir et al. (2006), as shown in Fig. 1a. For clarity, N6 and E6 are the designations used for the glass coupons oriented towards North and East with 15° inclination regarding the horizontal position, respectively. In ELAIA a single glass coupon was deployed on a single-axis tracking PV system, approximately 1.5 m above the ground, in a structure that replicates the usual PV module assembly glass-metal frame, see Fig. 1b. Weekly mass measurements were done to all 25 samples at PECS and monthly Scanning Electron Microscopy (SEM) and Energy Dispersive X-ray Spectroscopy (EDS) measurements were done to selected coupons from PECS and ELAIA. Mass was obtained using a Bosch SAE 80/200 microbalance model and the testing campaign started in the end of January 2017. The mass measurement uncertainty, 0.17 mg, was determined from several measurements of a clean glass. The objective is to study the mass accumulation on the glass coupons and relate it with the environmental conditions as well as to characterize the soiling accumulated. Mass accumulation on week t,$m_a(t)$, is determined by subtracting from the measured mass at that week, mass (t), the initial mass of the clean glass, mass(0):

$$m_a(t) = \text{mass}\ (t) - \text{mass}\ (0). \tag{1}$$

No cleaning is done to the glass during the experiment and only environmental action (e.g., rain) can act towards reducing the mass accumulated on the coupons.

2.2. PV performance

The testing campaign, related to the evaluation of the PV performance, being conducted since 31st October 2016 in PECS, is depicted in Fig. 1c. It shows two mc-Si PV flat panels of the same model FTS-220P, manufactured by Fluitecnik. The current-voltage (I-V) characteristic curves were obtained with a Eurotest PV Lite MI 3109 manufactured by Metrel. On these PV modules, one was manually cleaned before each I-V curve tracing and the other was kept unclean since the begining of the experiment. Three I-V curves were obtained for each module. The measurements were only performed in clear sky, near solar noon, and the tracker was always set perpendicular to the sun when performing the measurements. When not performing measurements, the panels are set facing south and tilted 30° from the horizontal. This is done to represent what would be the approximate position of a real fixed system, optimized for this location. This experiment is based fundamentally on Gostein et al. (2015), with one main difference: measurements are not taken continuously, so the number of points which contribute to the calculations is much smaller. The Soiling Ratio index (SR) is calculated by comparison of the short-circuit current (I_{SC}), which is denoted ($SR_{I_{SC}}$) and the maximum power output, (P_{max}), denoted ($SR_{P_{max}}$) of the two photovoltaic panels. The main difference noted in Gostein et al. (2015) is the fact that when soiling is homogeneous both metrics give similar results, but when the soiling is not homogeneous, calculating the soiling ratio based on the short circuit current can give either an underestimated or overestimated result, comparing it what was actually lost in power output. The reason for this is the fact that non-uniform soiling distorts the I-V curve in such a way that in some cases it changes considerably the I-V maximum power point. In mathematical terms, ($SR_{I_{SC}}$) and ($SR_{P_{max}}$) are calculated through Eqs. (2)–(4):

$$SR_{I_{SC}} = \frac{I_{SC}^{soil}}{I_{SC}^{soil,0}[1 + \alpha(T_{soil} - T_0)](G/G_0)}, \tag{2}$$

where I_{SC}^{soil} is the short-circuit current of the soiled PV panel, $I_{SC}^{soil,0}$ is the short-circuit current of the soiled PV at clean condition in Standard Test Conditions (STC), α is the short-circuit temperature correction coefficient, T_{soil} is the cell temperature of the soiled panel, T_0 is the temperature at reference condition (25 °C), G is the irradiance in the PV plane and G_0 the irradiance at STC conditions (1000 W/m^2).

$$SR_{P_{max}} = \frac{P_{max}^{soil}}{P_{max}^{soil,0}[1 + \gamma(T_{soil} - T_0)](G/G_0)}, \tag{3}$$

where P_{max}^{soil} is the maximum power of the dirty PV panel, $P_{max}^{soil,0}$ is the maximum power at clean condition and γ is the maximum power temperature correction coefficient. For the calculation of the irradiance in the PV plane, the clean module is used:

$$G = G_0 \frac{I_{SC}^{clean}[1 - \alpha(T_{clean} - T_0)]}{I_{SC}^{clean,0}}, \tag{4}$$

where I_{SC}^{clean} is the short-circuit current of the clean PV panel, $I_{SC}^{clean,0}$ is the short-circuit current at clean condition in Standard Test Conditions (STC), α is the short-circuit temperature correction coefficient and T_{clean} is the cell temperature of the cleaned panel.

Fig. 1. Glass coupon supports: (a) glass tree in PECS; (b) glass sample support in ELAIA; (c) PECS soiling experiment.

3. Desert dust event characterization

3.1. Dust transport

True-color images taken by the Visible Infrared Imaging Radiometer Suite (VIIRS) instrument aboard the NOAA/NASA Suomi NPP satellite, see Fig. 2, show the February 2017 Saharan desert dust event. The low pressure system caused the transport of dust to Portugal and brought particles from the Saharan region to the locations where the experiments were ongoing. As a consequence of particle transportation, a dust cloud covered the sky resulting in very high aerosol optical depth (AOD) values, exceeding the threshold in (Elias et al., 2006) for desert dust events by almost 10 times. Just considering this, it is clear that it was a major event, since when small events happen the AOD values are much lower (Silva et al., 2016). This was the case for the second event that occurred latter on March 2017. Nevertheless, NASA images did not

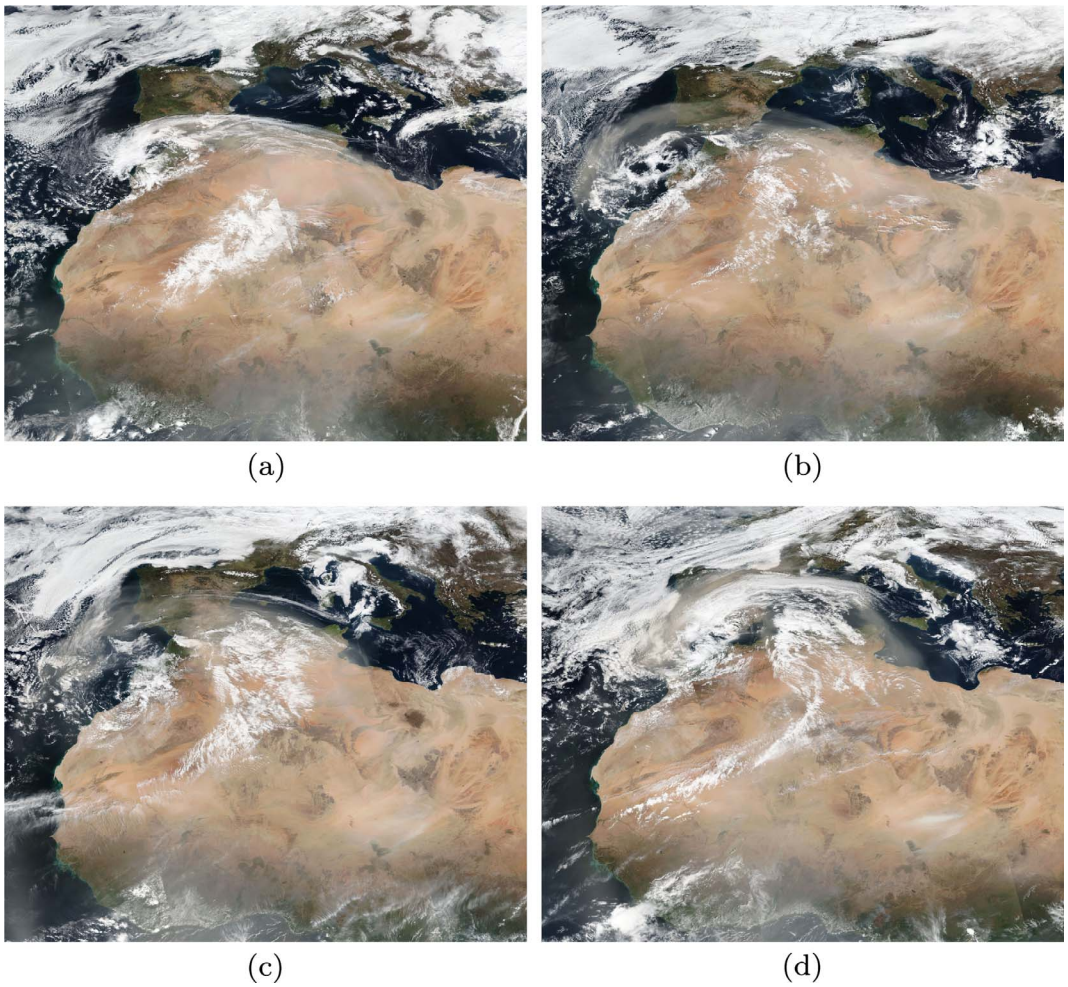

Fig. 2. NASA VSIIR dust event true image colors: (a) 20th February; (b) 21st February; (c) 22nd February; (d) 23rd February.

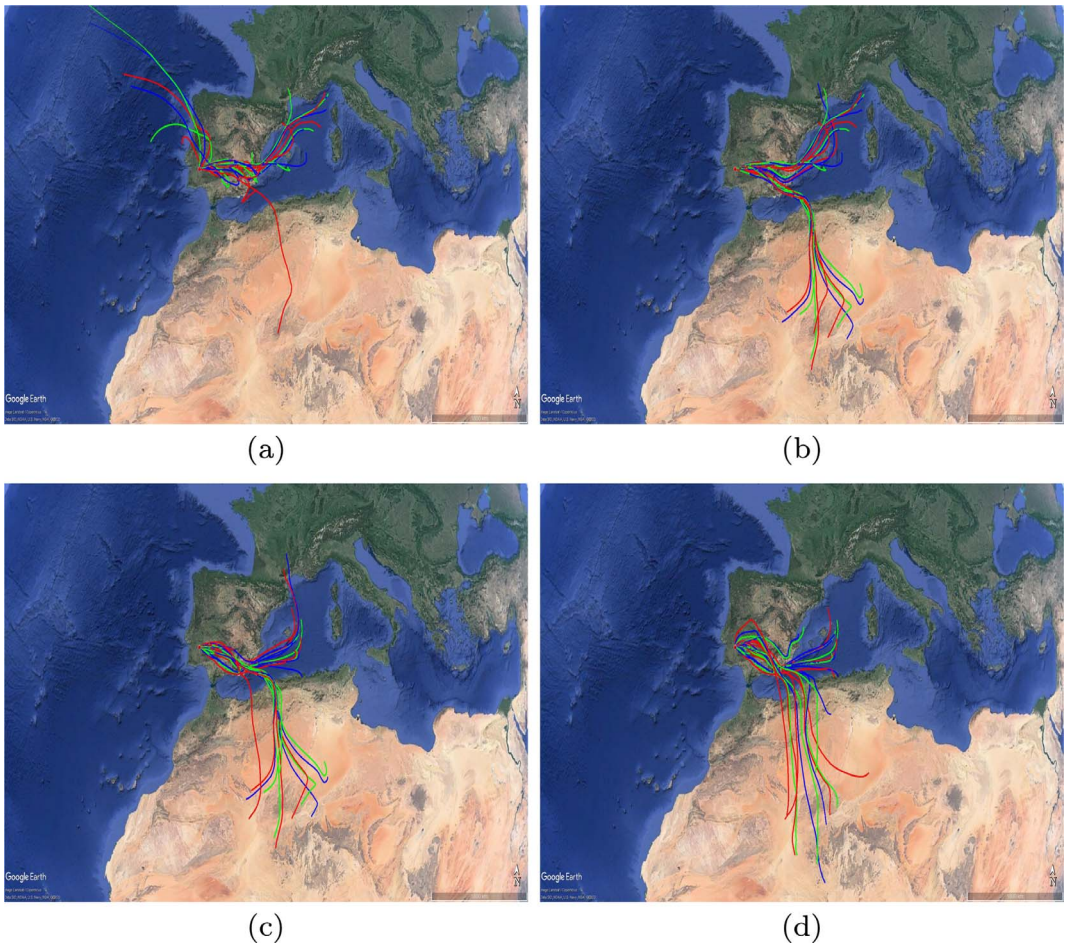

Fig. 3. HYSPLIT air masses trajectories: (a) 20th February; (b) 21st February; (c) 22nd February; (d) 23rd February.

allow the precise identification of the dust plume geographic point of origin and to obtain this information, the Hybrid Single-Particle Lagrangian Integrated Trajectory (HYSPLIT) modelling system (Stein et al., 2015) was used for the trajectory analysis, see Fig. 3. Backward trajectories were calculated from the NCEP Global Data Assimilation System (GDAS), (Kanamitsu, 1989), data with 0.5° by 0.5° latitude-longitude resolution. Trajectories were calculated every 2 h for a time frame of 48 h and the altitude at the desired location was set to 500 meters, which is enough for particle dry deposition or for it to be brought down by rain, in a process denoted as wet deposition. The different colors represent the different trajectories starting at each time step, although there are different trajectories with the same color since there are too many trajectories for the HYSPLIT color palette. From HYSPLIT analysis it is possible to conclude that dust plumes came mainly from North Mali, Algeria and Tunisia (all part of the Sahara desert), crossed the Mediterranean sea and reached Southern Europe.

To have further information on the amount of dust and the altitude at which the dust plume arrived at the experimental locations, the Barcelona Supercomputing Center (BSC) forecasts (Pérez et al., 2011; Haustein et al., 2012), were analysed (not shown). For the February event, the 21st was the day with the highest concentration, reaching approximately 900 $\mu g/m^3$ at 3 km altitude; in the next two days the concentration decreased until it reached background values on the third day. On the March event, the 15th had lower concentration values of 250 $\mu g/m^3$ again at 3 km altitude; the dust concentration decreased in the following days. According to data available in Wagner et al. (2009), background atmospheric aerosol load in May, in the region where both sites are located, is around 20 $\mu g/m^3$, but for February and March it is expected to be even less, since in May pollen concentration in the atmosphere increases, escalating the aerosol load. Thus, these forecasts show a 45-fold increase relative to background values on the February event, while in the March event there was a 5.25-fold increase, illustrating the clear difference between these two events.

3.2. Dust chemical analysis

The particles from the February dust event were deposited on the glass coupons in PECS, Fig. 1a, and in ELAIA, Fig. 1b. Two glass coupons from PECS, N6 and E6, were collected from the setup on the 22nd February, at the beginning of the dust break. N6 glass had multiple 'mud' drops, both visible under naked eye (Fig. 4a) and backscattered electron SEM (Fig. 4b). These were due to light rain contaminated with Saharan dust precipitated during the night of 21st February. The E6 glass coupon did not show the same drops, but it will be important for comparison between Saharan dust and local dust previously deposited on the glasses. The ELAIA glass was collected on the 23rd February. The three were analysed on the 25th February using SEM-EDS. It is assumed that the areas which were chosen to make the SEM-EDS analysis are representative of the entire glass surfaces. The ELAIA glass coupon, Fig. 4c, is mainly composed by aluminosilicates (AS) and halite (NaCl), see Fig. 4d with aluminium in blue, sulphur in green and chlorine in red. The AS are characteristic of desert areas, such as Sahara (Scheuvens et al., 2013; Kandler et al., 2007) and the NaCl probably resulted from the evaporation of sea spray collected by the dust plume while traveling over the Mediterranean sea (Lewandowska and Falkowska, 2013) and dragged together with the plume. The SEM image, Fig. 4c, shows particles of different sizes agglomerated. From the EDS analysis, Fig. 4d, it is seen that large particles, in red, correspond to

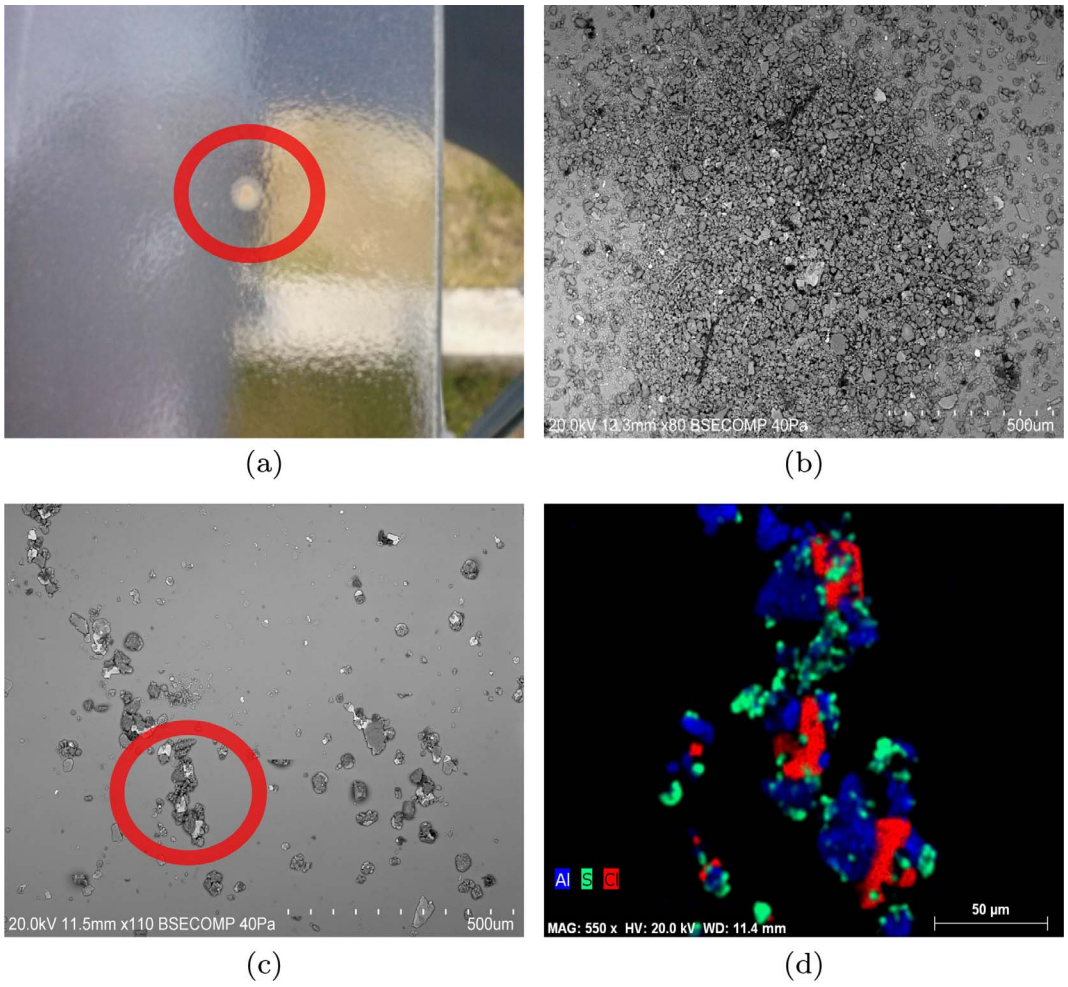

Fig. 4. PECS glass samples: (a) N6 rain drop with dust; (b) SEM of N6 glass rain drop. ELAIA glass sample; (c) SEM; (d) EDS of the zoomed structure.

NaCl. For PECS, the E6 sample (less affected by the dust event) showed AS, but also quartz (SiO_2) and calcite ($CaCO_3$), while N6 (with the 'mud' drop) showed quartz, iron oxides (Fe_yO_x), calcite, gypsum ($CaSO_4.2H_2O$), and rutile (TiO_2). Another important fact is that E6 glass had most particles spread and not agglomerated like the one from ELAIA and N6, possibly indicating agglomeration during the dust plume transport by particle collision. Regarding the dust point of origin, HYSPLIT points towards the Southern Algeria and northern Mali crossing northern Algeria and Tunisia. Following the procedure in Scheuvens et al. (2013), weight percentage (wt.%) ratios of (Ca + Mg)/Fe were calculated, since they can serve as indicators to differentiate locations for the Saharan dust. For ELAIA the value 1.89 was found, while for PECS, E6 and N6, the values were 3.21 and 2.23, respectively. Corresponding values for origin locations, Scheuvens et al. (2013), are in the range 0.62–2.08. While for N6 and ELAIA there is a reasonable agreement with the literature values, for E6 (which did not get hit by mud drops) the values are higher, probably due to the influence of the composition of local particles.

4. Results

4.1. Mass accumulation

The top-horizontal glass coupon at PECS in the week before the February event weighed 76.78376 g, at the event its mass was 76.79432 g and a week after 76.78388 g. This corresponds to an increase in the accumulated mass of almost $\approx 1067\ mg/m^2$; this is the highest mass accumulation during one week detected in this study, except for bird drops. The ELAIA sample weighed 76.96808 g right after the event, while cleaned it weighed 76.96410 g; which corresponds to an increase in mass accumulation of only $\approx 402\ mg/m^2$, a decrease of $665\ mg/m^2$ in relation to PECS. This difference can be related to the location, since the glass sample at ELAIA is surrounded by olive trees and by the 140 kWp PV plant (part of MASLOWATEN), while in PECS is a wide open experimental facility; both trees and the PV panels can work as a barrier to the dust brought from afar explaining the lower mass accumulation in ELAIA when compared to PECS. Nevertheless in the scenario of such intense soiling events, these barriers tend to have little effect, especially in the February event, in which most of the dust was brought down by rain; affecting equally both installations. Moreover, for March dust event the PECS glass mass was 76.78410 g the week before the event, 76.78669 g at the week of the event and 76.78306 g the week after the event, corresponding to an increase of $\approx 367\ mg/m^2$. At ELAIA, the sample was only measured on the 9th April; this was a week with a high pollen concentration according to the *Rede Portuguesa de Aerobiologia* (Portuguese Network of Aerobiology). The mass measured was 76.97520 g; which regarding the measurement from February's event corresponds to an increase of $\approx 720\ mg/m^2$. This increase is certainly not only due to the dust event (it rained after that), but due to the pollen concentration. The olive trees which acted as a barrier in the February event, were at that moment at the blossoming stage, being an active source of pollen, visible in posterior SEM images (April 2017) of the analysed samples. Regarding the aerosol optical thickness (*AOD*), defined as the integrated extinction coefficient over a vertical column of unit cross section, is represented in Fig. 5a for the 870 nm wavelength, which is the one usually used to identify situations as dust events (Elias

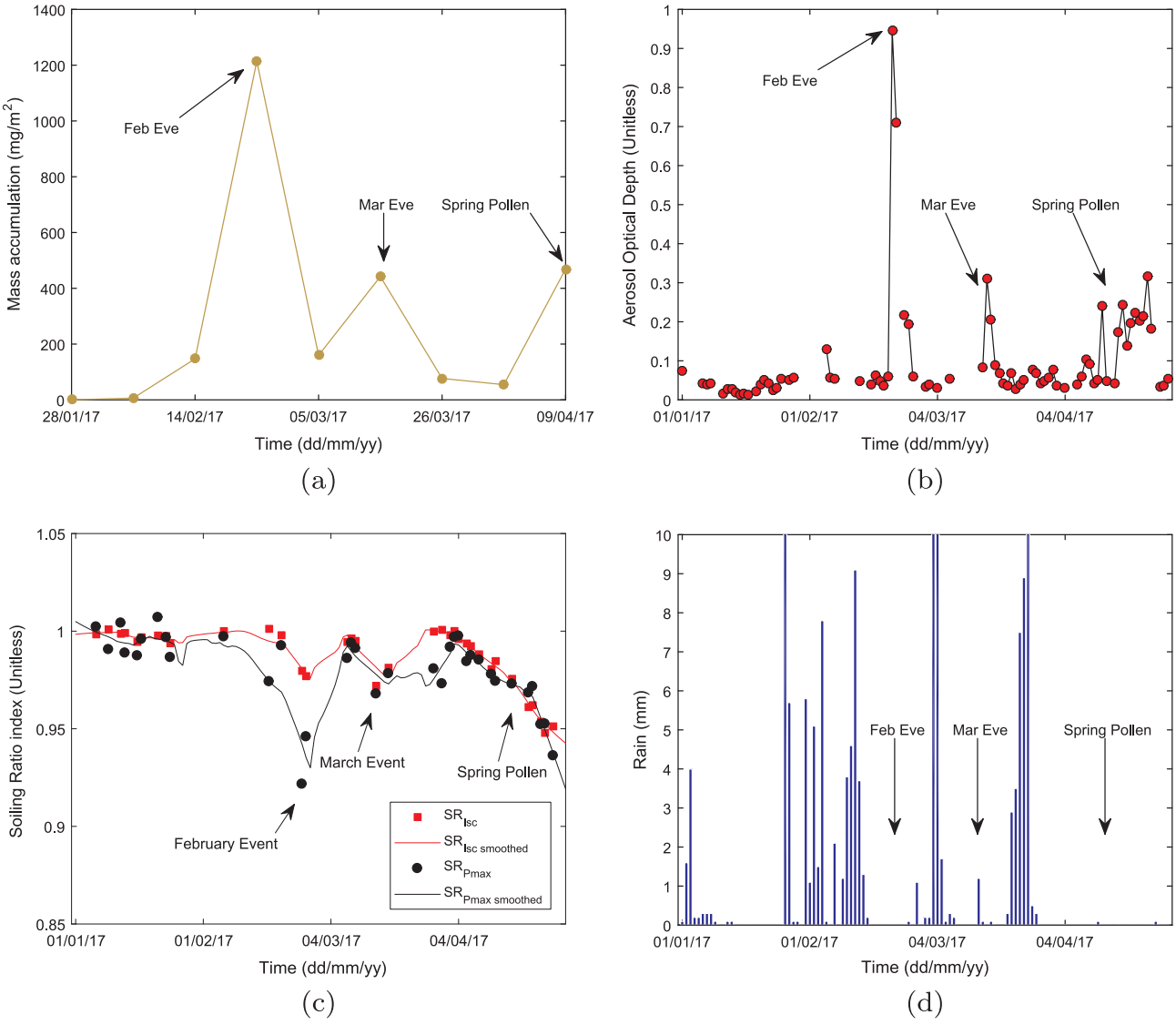

Fig. 5. PECS soiling experiment results: (a) mass accumulation; (b) AOD; (c) SR index; (d) precipitation.

et al., 2006). It can be seen that the two dust events, one in February and the other in March, have different *AOD* amplitudes. The February event has the highest one as expected, since the atmospheric particle concentration was higher. These measurements were taken at the University of Évora campus in the city centre (about 8 km away from PECS) and it also evidences that high *AOD* values on April are due to higher pollen concentration.

4.2. Photovoltaic performance

In Fig. 5c both SR metrics, $SR_{I_{SC}}$ in red dots and $SR_{P_{max}}$ in black dots, are presented; the corresponding lines evidence the general data trend. It highlights both dust events intermediated by rain, Fig. 5d, and April with basically no rain. Pollen influence on PV performance is shown in Fig. 5b, however is not to be addressed in the paper. Apart from these facts, when soiling is absent it is expected that both metrics have values close to one (not exactly one due to experimental errors and second order effects, (Dunn et al., 2013)); which is what happens here. More importantly, on the 25th February a significant decrease of 8% was obtained in the PV modules maximum power output and a decrease of only 3% in the short-circuit current. The reduction difference is due to the non-uniform particle deposition (Lorenzo et al., 2014) on the glass of the PV modules; as it was caused by light rain during the 21st February night. This points to $SR_{P_{max}}$ being more accurate metric for soiling; as noticed by Gostein et al. (2015). Most importantly, it warns the significant impact that dust events can have on the PV energy yield, mainly, taking into account that 4–5 major dust events tend to occur per year (Flentje et al., 2015). During the period of 14th–16th March, another event took place, but it was far less significant than the February event, mainly because the dust concentration and event duration were lower, as concluded from the BSC vertical profiles forecasts. Despite this fact, it had an effect of ≈3% decrease in both $SR_{I_{SC}}$ and $SR_{P_{max}}$, indicating homogeneous soiling. Soiling homogeneity may have been achieved through dry deposition and favorable atmospheric conditions and/or condensation during the nights.

5. Discussion

To detail the SR metrics plot performed at PECS, Fig. 5c, an environmental parameter analysis is required and for that, the most important variables regarding soiling are represented in Fig. 6. The dew point temperature in Fig. 6a, calculated with Magnus formula and NOAA parameters, indicates when the conditions for condensation to form are met. It can be seen from Fig. 6a that those conditions exist on most nights and from further site observations, it can be stated that condensation is frequent, mainly during the first two months of the

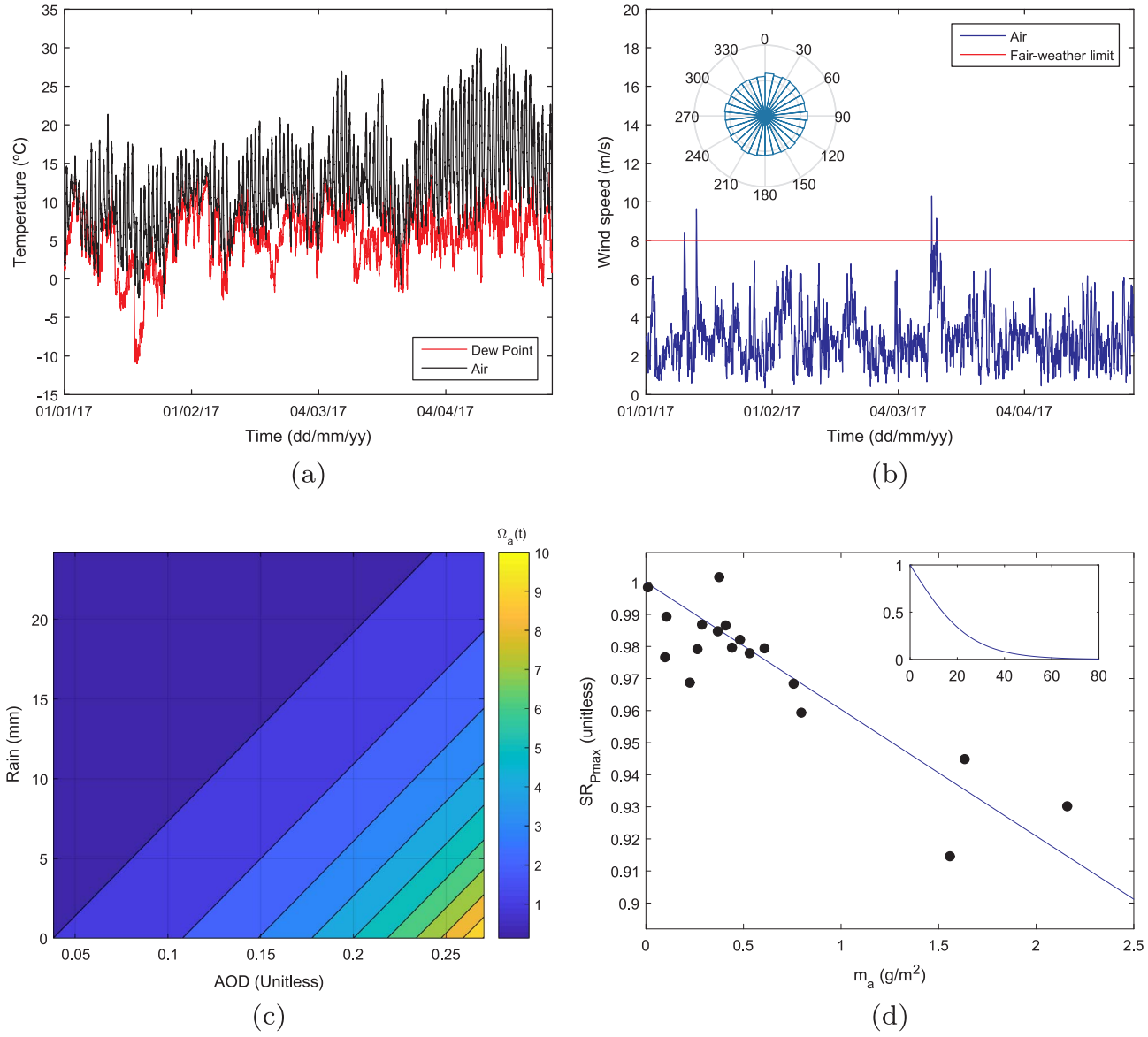

Fig. 6. Environmental parameters and modelling from January to April 2017: (a) air and dew point temperature; (b) wind speed and direction; (c) mass accumulation modelling; (d) SR modelling.

year. As also stated in Gostein et al. (2014) dew can help clean the surfaces and that along with frequent precipitation leads to SR constantly close to unity, however frequent humid/dry cycles like dew at night and high temperatures during the day may enhance the cementation process. With the air temperature rising and relative humidity lowering towards the summer, the probability for dew to form and for rain diminishes. In April, grains of pollen have time to build up on top of the PV modules leading to a decrease in both SR metrics; that is why it is very important to take into account not only the dust events but also pollen. Regarding wind speed Fig. 6b, the red horizontal line represents the 8 m/s limit hourly mean data (this value is usually used, see Harrison (2012), to define fair-weather conditions in atmospheric sciences). The higher the wind speed the more deposition will occur (Goossens and Van Kerschaever, 1999), which is in line with the general dust sedimentation model developed in Goossens (1988). Since there is no clean-cut air velocity threshold or limit to state at which point particle deposition can be greatly increased, the 8 m/s limit is used. From the data, it was calculated the amount of points which are below this limit and the value obtained was 99.6%. That together with precipitation and dew, forms a scenario not prone to soiling. Another important variable is the wind direction, inset in Fig. 6b. The wind did not have a dominant direction during the campaign. Nevertheless, previous observations indicated that dominant winds were from the North-East quadrant, which may increase soiling, since there is an active quarry a few kilometres east of PECS. Further studies (not presented here) were also performed to check if there was any variation from nocturnal winds to diurnal ones, but the same pattern was found on both situations.

Additionally it is possible to relate m_a (connected to the PV performance degradation) with the environmental parameters *RAIN* and *AOD*. The horizontal top glass at the PECS experiment was chosen to this study. Since m_a is measured almost every week, this time period is used to calculate total *RAIN* and mean *AOD* for each measurement point; this last variable is not sampled regularly and only during day time and in the absence of clouds/precipitation. Note that the variable *RAIN*corresponds to the sum of the precipitation during a given week. Ideally, particle counter measurements should be more appropriate than *AOD*, but no such equipment was available at the time. In these conditions, an empirical model is proposed to relate *AOD* and *RAIN* of a given week *t* with the ratio of the m_a for that week with the previous

one, as expressed by:

$$\Omega_a(t) = \frac{m_a(t)}{m_a(t-1)} = \Omega_0 \exp[\omega_1 AOD(t) - \omega_2 RAIN(t)], \quad (5)$$

where $\Omega_0 = 0.6833$ with 95% confidence bounds (0.4692, 0.8974) (unitless), $\omega_1 = 9.948$ with 95% confidence bounds (8.664, 11.230) (unitless) and $\omega_2 = 0.0868$ with 95% confidence bounds (0.0119, 0.1559) (mm^{-1}). Taking into account a complete series (without bird drops) this model fits well the data, see Fig. 6c: $r^2 = 0.95$ and adjusted $r^2 = 0.95$; indicating that both variables are contributing to the model, while the RMSE is 0.772. For the *AOD* a positive exponential is applied, while for the *RAIN* a negative one is used. Moreover, Ω_0 represents the background contribution to soiling arising from particles not detected by the *AOD* measurements. A more accurate analysis would, in fact, need to take particle size distributions into account. Furthermore, the model respects two important asymptotic limits, which are: $\lim_{RAIN\to\infty}\Omega_a = 0$ and $\lim_{AOD\to\infty;RAIN\to 0}\Omega_a = \infty$. Although these limits will never be reached, they are in line with the most basic idea behind soiling, which is: if there is rain and low concentration of particles in the atmosphere, the amount of deposition will be low; nevertheless if the amount of rain is low and the amount of particles is high, the deposition will increase. It should be said that the use of a small time frame, like the one used here, contributes to the stability of the model. Using a larger time frame may result in a certain loss of sensitivity of the model because the values and periodicity of *AOD* and *RAIN* for larger time periods may ruin any possible relation. To complete the analysis, a simple model was used to relate m_a with the SR_{Pmax}, (for both homogeneous and non-homogeneous soiling), and can be seen in Fig. 6d. It is given by Eq. (6):

$$SR_{P_{\max}}(m_a) = \frac{2}{1 + \exp(m_a/m_0)}. \quad (6)$$

For this model, Fig. 6d, a $r^2 = 0.7$ (with the same adjusted r^2) was obtained, with a characteristic mass: $m_0 \approx 12.61\ g/m^2$ with 95% confidence bounds (10.40, 14.81). This model represents a steep descending in $SR_{P_{\max}}$ at the beginning until it stabilizes resembling transmittance measurements (John et al., 2016). Actually, the model estimates near zero $SR_{P_{\max}}$ values with a critical mass density m_c around $75\ g/m^2$, Fig. 6d inset; which is in line with literature values (John et al., 2016) for glass transmittance losses. Similarly to the previous model this empirical relation captures the essential asymptotic behaviours: $\lim_{m_a\to\infty} SR_{P_{\max}} = 0$ and $\lim_{m_a\to 0} SR_{P_{\max}} = 1$, these are the completely soiled and completely clean limits, respectively.

6. Conclusions

The results presented in this study demonstrate several important points: (i) particles from a remote origin have a significant role in soiling and it shows that soiling is not only a consequence of local phenomena; (ii) the need to forecast long-range dust transport and its impact; (iii) soiling rate may not be always linear, as some prediction models assume; (iv) exponential empirical models describe well the relation of mass accumulation and the environmental parameters. Note that more data points are needed to assess the model robustness, and to test data from locations with other climates, to see if the model holds; however this is a preliminary model and its potential resides in the fact of using only two variables. This study clearly shows the negative effect of the Saharan dust events on the southern Iberian peninsula (thousands of kilometres away from point of origin), with a significant decrease in the production of photovoltaic energy due to soiling and significant economic effects on solar energy installations (especially in low rain seasons). It also highlights the need for the development of low-cost soiling mitigation tools like anti-soiling coatings.

Acknowledgements

This research has received funding from H2020 MASLOWATEN European project with the ID 640771, which all authors acknowledge. This work was co-funded by the European Union through the European Regional Development Fund, framed in COMPETE 2020 (Operational Programme Competitiveness and Internationalisation) through ICT (UID/GEO/04683/2013) with reference POCI-01–0145-FEDER-007690 and DNI-ALENTEJO with reference ALT20-30–0145-FEDER-000011. Ricardo Conceição also acknowledges the FCT scholarship SRFH/BD/116344/2016. Hugo Silva is grateful to DNI-ALENTEJO and INSHIP (H2020-LCE-2016-ERA) projects. The authors gratefully acknowledge the NOAA Air Resources Laboratory for the provision of the HYSPLIT rransport and dispersion model and READY website (http://www.ready.noaa.gov) used in this publication and also to NOAA/NASA for the true color satellite images. The authors also gratefully acknowledge the Hercules Laboratory for the SEM-EDS analysis. The authors acknowledge the Barcelona Supercomputing Center for their NMMB/BSC-Dust model (http://www.bsc.es/ESS/nmmb_bsc-dust).

References

Appels, R., Lefevre, B., Herteleer, B., Goverde, H., Beerten, A., Paesen, R., De Medts, K., Driesen, J., Poortmans, J., 2013. Effect of soiling on photovoltaic modules. Sol. Energy 96, 283–291.

Dunn, L., Littmann, B., Caron, J.R., Gostein, M., 2013. PV module soiling measurement uncertainty analysis. In: 2014 IEEE 40th Photovoltaic Specialist Conference (PVSC), IEEE, pp. 0658–0663.

El-Shobokshy, M.S., Hussein, F.M., 1993. Effect of dust with different physical properties on the performance of photovoltaic cells. Sol. Energy 51 (6), 505–511.

Elias, T., Silva, A.M., Belo, N., Pereira, S., Formenti, P., Helas, G., Wagner, F., 2006. Aerosol extinction in a remote continental region of the Iberian Peninsula during summer. J. Geophys. Res. 111.

Elminir, H.K., Ghitas, A.E., Hamid, R., El-Hussainy, F., Beheary, M., Abdel-Moneim, K.M., 2006. Effect of dust on the transparent cover of solar collectors. Energy Convers. Manage. 47, 3192–3203.

Flentje, H., Briel, B., Beck, C., Collaud Coen, M., Fricke, M., Cyrys, J., Gu, J., Pitz, M., Thomas, W., 2015. Identification and monitoring of Saharan dust: an inventory representative for south Germany since 1997. Atmos. Environ. 109, 87–96.

Goossens, D., 1988. The effect of surface curvature on the deposition of loess: a physical model. Catena 15 (2), 179–194.

Goossens, D., Van Kerschaever, E., 1999. Aeolian dust deposition on photovoltaic solar cells: the effects of wind velocity and airborne dust concentration on cell performance. Sol. Energy 66 (4), 277–289.

Gostein, M., Caron, J.R., Littmann, B., 2014. Measuring soiling losses at utility-scale PV power plants. In: 2014 IEEE 41st Photovoltaic Specialist Conference (PVSC). IEEE, pp. 0885–0890.

Gostein, M., Duster, T., Thuman, C., 2015. Accurately measuring PV soiling losses with soiling station employing module power measurements. In: 2014 IEEE 42nd Photovoltaic Specialist Conference (PVSC). IEEE, pp. 1–4.

Harrison, R., 2012. Aerosol-induced correlation between visibility and atmospheric electricity. J. Aerosol Sci. 52, 121–126.

Haustein, K., Pérez, C., Baldasano, J.M., Jorba, O., Basart, S., Miller, R.L., Janjic, Z., Black, T., Nickovic, S., Todd, M.C., Washington, R., Müller, D., Tesche, M., Weinzierl, B., Esselborn, M., Schladitz, A., 2012. Atmospheric dust modeling from meso to global scales with the online NMMB/BSC-Dust model –Part 2: Experimental campaigns in Northern Africa. Atmosph. Chem. Phys. 12 (6), 2933–2958.

Horta, P., Osório, T., Marcha, J., Collares-Pereira, M., 2015. ESCTP: Évora solar concentrators testing platform. In: SolarPACES, pp. 130010-1–130010-6.

John, J.J., Warade, S., Tamizhmani, G., Kottantharayil, A., 2016. Study of soiling loss on photovoltaic modules with artificially deposited dust of different gravimetric densities and compositions collected from different locations in India. IEEE J. Photovolt. 6 (1), 236–243.

Kanamitsu, M., 1989. Description of the NMC global data assimilation and forecast system. Wea Forecast. 4, 235–342.

Kandler, K., Benker, N., Bundke, U., Cuevas, E., Ebert, M., Knippertz, P., Rodríguez, S., Schütz, L., Weinbruch, S., 2007. Chemical composition and complex refractive index of Saharan Mineral Dust at Izaña, Tenerife (Spain) derived by electron microscopy. Atmos. Environ. 41 (37), 8058–8074.

Kazmerski, L.L., Diniz, A.S.A., Maia, C.B., Viana, M.M., Costa, S.C., Brito, P.P., Campos, C. D., de Morais Hanriot, S., de Oliveira Cruz, L.R., 2016. Soiling particle interactions on PV modules: surface and inter-particle adhesion and chemistry effects. In: 2016 IEEE 43rd Photovoltaic Specialists Conference (PVSC). IEEE, pp. 1714–1717.

Lewandowska, A.U., Falkowska, L.M., 2013. Sea salt in aerosols over the southern baltic. Part 1. The generation and transportation of marine particles**parts of this paper were originally published in polish: Lewandowska a., 2011, chemizm aerozoli w rejonie zatoki gdańskiej, wyd. ug, gdańsk, 184pp. Oceanologia 55(2), 279–298.

Lopes, F., Silva, H., Salgado, R., Cavaco, A., Canhoto, P., Collares-Pereira, M., 2017. Short-term ECMWF forecasts of solar irradiance for solar energy systems validated in

southern portugal. Sol. Energy (in preparation).
Lorenzo, E., Moretón, R., Luque, I., 2014. Dust effects on PV array performance: in-field observations with non-uniform patterns: dust effects on PV array performance. Prog. Photovolt. Res. Appl. 22 (6), 666–670.
Mallineni, J., Yedidi, K., Shrestha, S., Knisely, B., Tatapudi, S., Kuitche, J., TamizhMani, G., 2014. Soiling losses of utility-scale PV systems in hot-dry desert climates: results from four 4–16 years old power plants. In: 2014 IEEE 40th Photovoltaic Specialist Conference (PVSC). IEEE, pp. 3197–3200.
Mejia, F.A., Kleissl, J., 2013. Soiling losses for solar photovoltaic systems in California. Sol. Energy 95, 357–363.
Pérez, C., Haustein, K., Janjic, Z., Jorba, O., Huneeus, N., Baldasano, J.M., Black, T., Basart, S., Nickovic, S., Miller, R.L., Perlwitz, J.P., Schulz, M., Thomson, M., 2011. Atmospheric dust modeling from meso to global scales with the online NMMB/BSC-Dust model – Part 1: Model description, annual simulations and evaluation. Atmosph. Chem. Phys. 11 (24), 13001–13027.
Sayyah, A., Horenstein, M.N., Mazumder, M.K., 2014. Energy yield loss caused by dust deposition on photovoltaic panels. Sol. Energy 107, 576–604.
Scheuvens, D., Schütz, L., Kandler, K., Ebert, M., Weinbruch, S., 2013. Bulk composition of northern African dust and its source sediments – a compilation. Earth-Sci. Rev. 116, 170–194.
Sheffield, J., Goteti, G., Wood, E.F., 2006. Development of a 50-year high-resolution global dataset of meteorological forcings for land surface modeling. J. Clim. 19 (13), 3088–3111.
Silva, H., Lopes, F., Pereira, S., Nicoll, K., Barbosa, S., Conceição, R., Neves, S., Harrison, R., Collares Pereira, M., 2016. Saharan dust electrification perceived by a triangle of atmospheric electricity stations in Southern Portugal. J. Electrost. 84, 106–120.
Smith, W.H., 1977. Removal of atmospheric particulates by urban vegetation: implications for human and vegetative health. Yale J. Biol. Med. 50 (2), 185.
Stein, A.F., Draxler, R.R., Rolph, G.D., Stunder, B.J.B., Cohen, M.D., Ngan, F., 2015. NOAA's HYSPLIT atmospheric transport and dispersion modeling system. Bull. Am. Meteorol. Soc. 96 (12), 2059–2077.
Šúri, M., Huld, T.A., Dunlop, E.D., Ossenbrink, H.A., 2007. Potential of solar electricity generation in the European Union member states and candiyear countries. Sol. Energy 81 (10), 1295–1305.
Thrasher, B., Maurer, E.P., McKellar, C., Duffy, P.B., 2012. Technical note: bias correcting climate model simulated daily temperature extremes with quantile mapping. Hydrol. Earth Syst. Sci. 16 (9), 3309–3314.
Wagner, F., Bortoli, D., Pereira, S., Costa, M.J., Silva, A.M., Weinzierl, B., Esselborn, M., Petzold, A., Rasp, K., Heinold, B., Tegen, I., 2009. Properties of dust aerosol particles transported to Portugal from the Sahara desert: aerosol properties of mineral particles. Tellus B 61 (1), 297–306.